Microchimica Acta (2019) 186: 533
https://doi.org/10.1007/s00604-019-3639-7

ORIGINAL PAPER

Stamped multilayer graphene laminates for disposable in-field electrodes: application to electrochemical sensing of hydrogen peroxide and glucose

Loreen R. Stromberg[1] · John A. Hondred[1] · Delaney Sanborn[1] · Deyny Mendivelso-Perez[2] · Srikanthan Ramesh[3] · Iris V. Rivero[3] · Josh Kogot[4] · Emily Smith[2] · Carmen Gomes[1] · Jonathan C. Claussen[1]

Received: 10 January 2019 / Accepted: 26 June 2019 / Published online: 15 July 2019

Abstract

A multi-step approach is described for the fabrication of multi-layer graphene-based electrodes without the need for ink binders or post-print annealing. Graphite and nanoplatelet graphene were chemically exfoliated using a modified Hummers' method and the dried material was thermally expanded. Expanded materials were used in a 3D printed mold and stamp to create laminate electrodes on various substrates. The laminates were examined for potential sensing applications using model systems of peroxide (H_2O_2) and enzymatic glucose detection. Within the context of these two assay systems, platinum nanoparticle electrodeposition and oxygen plasma treatment were examined as methods for improving sensitivity. Electrodes made from both materials displayed excellent H_2O_2 sensing capability compared to screen-printed carbon electrodes. Laminates made from expanded graphite and treated with platinum, detected H_2O_2 at a working potential of 0.3 V (vs. Ag/AgCl [0.1 M KCl]) with a 1.91 μM detection limit and sensitivity of 64 $nA{\cdot}\mu M^{-1}{\cdot}cm^{-2}$. Electrodes made from platinum treated nanoplatelet graphene had a H_2O_2 detection limit of 1.98 μM (at 0.3 V), and a sensitivity of 16.5 $nA{\cdot}\mu M^{-1}{\cdot}cm^{-2}$. Both types of laminate electrodes were also tested as glucose sensors via immobilization of the enzyme glucose oxidase. The expanded nanographene material exhibited a wide analytical range for glucose (3.7 μM to 9.9 mM) and a detection limit of 1.2 μM. The sensing range of laminates made from expanded graphite was slightly reduced (9.8 μM to 9.9 mM) and the detection limit for glucose was higher (18.5 μM). When tested on flexible substrates, the expanded graphite laminates demonstrated excellent adhesion and durability during testing. These properties make the electrodes adaptable to a variety of tests for field-based or wearable sensing applications.

Keywords Nanomaterials · Nanotechnology · Biosensing · In-field sensors · Flexible electrodes · Scalable manufacturing

Electronic supplementary material The online version of this article (https://doi.org/10.1007/s00604-019-3639-7) contains supplementary material, which is available to authorized users.

✉ Jonathan C. Claussen
jcclauss@iastate.edu

[1] Department of Mechanical Engineering, Iowa State University, Ames, Iowa 50011, USA

[2] Department of Chemistry, Iowa State University, Ames, Iowa 50011, USA

[3] Department of Industrial and Systems Engineering, Rochester Institute of Technology, Rochester, New York 14623, USA

[4] Science and Technology Department, Naval Surface Warfare Center, Panama City, Florida 32407, USA

Introduction

Low-cost graphene electrodes that are flexible and/or degradable are important for a wide variety of applications including wearable health monitoring, medical implants, and environmental sensors. However, printable inks for the scalable manufacturing of graphene-based electrodes require the use of non-conductive binders and post-print annealing steps which hinders electrical conductivity, thereby reducing sensor performance and increasing manufacturing complexity. Electrochemical sensors are quickly becoming an essential commodity for medical professionals, patients, researchers, farmers, and anyone that interacts with the modern world, as sensors have thousands of applications and have become heavily integrated into daily lives [1].

However, despite many promising discoveries in disease detection, foodborne pathogen sensing, as well as plant and animal health monitoring, biosensors fail to be commercialized for many reasons. One of these pitfalls is the cost of single-use electrodes for electrochemical sensing [2]. Electrodes can be generated from a plethora of pure or composite conductive materials. To lower production costs, researchers and industry have used many scalable manufacturing techniques to print electrodes using conductive inks. However, the inks are often comprised of metals such as silver, gold, and platinum [3, 4] which increases cost per test. To reduce costs of mass production, many researchers have turned to graphene and its derivative material graphite because of lower costs and intrinsic physical properties that make it a good candidate for electrochemical testing [5, 6]. Graphite is a stack of 2D layers of planar crystalline carbon atoms, with bulk graphite having a 3D nature. Between the planes exist weak Van der Waals bonds that enable the formation of multi-layer graphene (referred to as graphite). Graphitic materials are stable at high temperatures, possess high tensile strength, are chemically inert, and are excellent conductors of both heat and electricity [7]. These characteristics make carbon-based materials promising candidates for electrochemical sensors, which require high conductivity to maximize sensitivity during electrochemical sensing [8, 9].

Graphene, and graphene-like materials can be used for a multitude of sensing applications. While it has been documented that neither material alone is the most efficient platform for direct detection of glucose or detection of H_2O_2 [6], they remain important base components or scaffolds for metal-based catalysts in electrochemical sensor applications [10–12]. As such, many graphene- or carbon- based electrochemical sensors have been evaluated using classical benchmark testing of H_2O_2 oxidation and detection of glucose (typically via the breakdown of glucose) [13, 14]. As these are critical analytes in both healthcare and industrial applications, highly sensitive assays (down to pico- and atto- molar concentrations) for their detection have been widely published [14, 15]. Since the oxidation of H_2O_2 can be readily detected at the electrode surface, many researchers have utilized carbon-based electrodes and/or electrodes further modified with platinum, gold, silver, nickel, and copper for monitoring glucose or H_2O_2 [16–19]. Additionally, a plethora of other surface modification and doping strategies have been investigated for improving detection of these analytes, and also as a means to further detection of other targets of interest [6, 20–23].

To avoid the high-cost, low-yield nature of traditional graphene fabrication, researchers have established numerous techniques to print circuit patterns using graphene-based inks [24, 25]. However, the inks typically require the use of non-conductive binders (e.g., ethyl cellulose or nitrocellulose) in order to increase graphene-substrate adhesion [26]. Moreover, these printing techniques require post-print annealing (e.g., thermal or photonic) to improve electrical conductivity by removing ink solvents, graphitizing non-conductive binders, and/or reducing graphene oxide flakes to graphene [27]. These printing and annealing techniques can be challenging or impossible to perform on textured, degradable/biodegradable or thermally sensitive surfaces where solution-phase graphene cannot properly adhere to the surface, or burning and degradation occurs during the annealing process. A potential alternative to solution-phase printing of graphene electrodes is the use of flexible, stamped multi-layer graphene laminates.

Flexible graphene laminates or foils have demonstrated excellent conductivity and can be molded or cut into differentf shapes and thicknesses for a wide variety of applications [28, 29]. Laminate sheets are generally comprised of a few to many layers of chemically grown graphene, followed by stacking of single sheets and rolling compression to laminate them together [28]. Alternatively, layers of binder-free graphene ink can be printed directly and then subjected to rolling compression to create laminates [30]. Multi-layer graphene laminates have been demonstrated in many sensor applications such as strain [31], humidity [32], and RFIDs [30]. However, use in biosensing has been limited to detection of electroactive species (ascorbic acid, dopamine and uric acid), which do not require functionalization with a biorecognition agent [33].

Stamped multi-layer graphene laminate electrodes on disposable and flexible substrates for electrochemical biosensing are a potential solution to creating graphene-based electrodes on fragile substrates. To examine physical and electrochemical properties, two distinct laminates were synthesized from expanded graphite (eGR) and expanded nanoplatelet graphene (nGN) and the electrochemical performance was evaluated using the model systems of H_2O_2 and glucose sensing. Materials for laminates were created via chemical exfoliation using a modified Hummers' method [34], followed by thermal expansion on a hot plate. The resulting expanded graphitic 'worms' [35] were loaded into a 3D-printed electrode-shaped mold and complementary stamp to create laminate electrodes on various substrates. Flexible materials tested as substrates included a heat stabilized polyethylene terephthalate (PET), flexible polyimide tape, and biodegradables (i.e. 2% chitosan films or polycaprolactone/agar composites). The surface topography, graphitic nature, and surface functional groups of the resulting laminates was analyzed using scanning electron microscopy (SEM), Raman spectroscopy, and x-ray photoelectron spectroscopy (XPS). The electrochemical behavior of bare, untreated eGR was compared to nGN and screen-printed carbon (SPC) electrodes and evaluated using cyclic voltammetry (CV) and electrochemical impedance spectroscopy (EIS) to determine the performance of the material. The amperometric response of eGR was evaluated using H_2O_2 sensing at different potentials (0.2, 0.3, 0.4, 0.5 V) and a working potential of 0.3 V was selected based on the sensing results and the CV data. To improve the

electrocatalytic nature of the laminates, platinum nanoparticles (PtNPs) were electrodeposited onto electrodes prior to testing with hydrogen peroxide (H_2O_2) and glucose [after covalent attachment of the enzyme glucose oxidase (GOx)]. The PtNPs improved the H_2O_2 sensing capabilities of the eGR and SPC electrodes, but more than a 4-fold reduction in signal was seen in the nGN electrodes. Thus, the H_2O_2 limits of detection (LoD) for electrodes with PtNPs was eGR < nGN < SPC, with eGR having the lowest limit of detection (1.91 μM) and the highest sensitivity (64.3 $nA \cdot \mu M^{-1} \cdot cm^{-2}$). In terms of glucose sensing, the nGN electrodes demonstrated the best results with a sensing range between 1.22 μM and 9.88 mM, and a limit of detection (LoD) of 1.22 μM. These values are within the normal physiological range (5 μM – 5 mM) for glucose found in blood [36], sweat [37], tears [38], and saliva [39]. The laminates made from eGR were able to detect 18.5 μM glucose with a sensing range up to 9.88 mM. Finally, the stability of the eGR laminate electrodes stamped onto various substrates was analyzed. Results demonstrated that the laminates were highly stable on smoother substrates such as the non-degradable PET and polyimide films, as well as the degradable polycaprolactone (PCL) and agar composites, but were unstable (delamination occurred) on hygroscopic chitosan-based substrates. This indicates that the laminates are a good candidate for low cost in-field applications as they can be fabricated on a variety of materials and still exhibit good stability and sensitivity in detection assays.

Experimental details

Materials

All chemicals were sourced from Sigma Aldrich and Fisher Scientific and were used without further purification or modification unless otherwise noted. Bulk graphite, chitosan, polycaprolactone, agar, glucose, 1-Ethyl-3-(3-dimethylaminopropyl)carbodiimide (EDC), N-Hydroxysuccinimide (NHS), 2-(N-morpholino)ethanesulfonic acid (MES), potassium ferricyanide, potassium ferrocyanide trihydrate, potassium chloride (KCl), glucose oxidase (GOx) from *Asperigillus niger*, and 10x phosphate buffered saline (PBS, catalog P5493) were sourced from Sigma Aldrich (www.sigmaaldrich.com). 10x PBS was diluted to a working concentration of 1x PBS (phosphate buffer [0.01 M], sodium chloride [0.154 M]) using deionized water and then filtered using a 0.2 μm filter. Acetic acid, hydrogen peroxide (H_2O_2), sulfuric acid, potassium permanganate, and phosphoric acid were purchased from Fisher Scientific (www.fishersci.com/us/en/home.html). Graphene powder and nanoplatelet graphene were purchased from ACS Material (www.acsmaterial.com).

Intercalation and thermal expansion of graphite

Graphite intercalation was performed with a modified Hummers' method described by Marcano et al. [34], using excess graphite or nanoplatelet graphene ((nGN) 2–10 nm thickness). Additional experimental details are provided in Electronic Supplementary Material (ESM) including three videos that show the rapid thermal expansion process of the sulfurintercalated graphite and the nanoplatlet graphite material. During intercalation and oxidation, the mixture was covered and refrigerated at 4 °C for 7 days, with daily stirring. Resulting sulfur-intercalated material was thoroughly washed until no discoloration of waste water was observed, then subjected to drying for 3 h at 120 °C. A small amount of the dried powder was placed into a pre-heated Pyrex dish on a 540 °C hot plate and allowed to fully expand.

Biodegradable substrate fabrication

Chitosan films were fabricated by dissolving 2% $w \cdot v^{-1}$ chitosan in acetic acid, overnight with continuous stirring. The solution was poured in 100 mm plastic petri dishes and evaporated inside of a chemical fume hood. Polycaprolactone (PCL) and agar (PCL:Agar) blends were produced by mixing 75:25 $w \cdot w^{-1}$ or 50:50 $w \cdot w^{-1}$ of PCL:Agar in a single-screw extruder (Filabot EX2, www.filabot.com) at 80 °C with active cooling as a 2.75 mm filament. The PCL:Agar substrates were printed at 120 °C using a Lulzbot Mini (www.lulzbot.com) equipped with a flexystruder head.

Electrode fabrication

A 3D electrode-shaped mold and corresponding stamp (Fig. S1) were designed in SolidWorks (www.solidworks.com) and printed on a Form2 3D printer (www.formlabs.com) using clear resin. Multiple types of substrates, such as PET (Kemafoil® TSL, www.coveme.com), flexible polyimide (Kapton®, www.kaptontape.com) tape, 2% $w \cdot v^{-1}$ chitosan films, and PCL/agar composites, were investigated to determine how the stamping method and resulting electrodes would perform on different materials. A video demonstrating the fabrication of the electrode is located in ESM. Unless stated otherwise, the substrate used is PET (Kemafoil® TSL polymer), and will henceforth be referred to only as PET. Substrates were sectioned, cleaned with ethanol (except chitosan films) and a sticker paper stencil was applied to minimize excess adhesive residue prior to application of a layer of 3M® multipurpose adhesive (video demonstration is seen in File S6, www.3m.com). The 3D printed mold was aligned and expanded graphitic materials were deposited into the mold and manual pressure was applied to compress the stamp and create an electrode. A nail polish resist layer was applied to electrodes to maintain a consistent electrochemical working

area. To measure mass of eGR used, electrodes were made with a water-soluble glue (Elmer's® School Glue Stick, www.elmers.com), submerged in deionized water for 10–15 min to dissolve adhesive, then air dried overnight and weighed on a microbalance (Fig. S2).

Electrode surface modifications

To perform electrodeposition, electrodes were placed in a platinizing solution (4 mM chloroplatinic acid and 0.5 M sodium sulfate) using a counter platinum gauze (52 mesh, www.beantownchem.com). A step current program on the potentiostat (www.chinstruments.com) was set at an applied current of 5 mA, with step time of 0.1 s, and 100 cycles. Oxygen plasma was used to pre-treat and clean the surface of the electrodes prior to biofunctionalization with glucose oxidase. Conditions for treatment were 10 psi, high RF level, for 5 min in a PDC-32G plasma cleaner with a Plasmaflo accessory (www.harrickplasma.com).

Biofunctionalization

To evaluate efficacy as a biosensor, the electrodes treated with PtNPs and oxygen plasma were functionalized with the enzyme GOx (glucose oxidase). The electrode surface was incubated for 30 min with 75 mM EDC + 25 mM NHS prepared in MES buffer, pH 6.0. The EDC/NHS mixture was removed from the electrode via pipet, and the surface rinsed with fresh MES buffer. 2 $mg{\cdot}mL^{-1}$ GOx prepared in MES buffer was incubated on the surface for 1 h, and then rinsed off with a 1x dilution of PBS (1x PBS) pH 7.4, prior to testing.

Scanning Electron microscopy

Scanning electron micrographs were used to visualize the surface roughness of the stamped laminate electrodes and the raw thermally expanded materials. Prior to imaging, 2 nm of Iridium was deposited using a turbo pump sputter coating device. A field emission scanning electron microscope (FEI Quanta 250) with a working distance of 10.0 mm, spot size of 3.0, and accelerating potential of 10 kV was used to capture all images.

Electrochemical testing

Cyclic voltammograms were collected in a redox solution of 4 mM potassium ferricyanide, 4 mM potassium ferrocyanide trihydrate, and 0.1 M KCl, using scan rates between 5 and 100 $mV{\cdot}s^{-1}$. Electrochemical impedance spectroscopy was performed in the same redox solution, using a three electrode setup (platinum wire counter, Ag/AgCl ref.), initial potential of 0.0 V, amplitude of 0.005 V, and sweeping from 10^6 to 10^3 Hz. Data were plotted as real impedance versus imaginary impedance. Amperometric testing of electrodes was performed using a standard 3 electrode set up. A potential of 0.3 V was applied and monitored using a Ag/AgCl reference electrode (0.1 M KCl) with a platinum wire counter electrode (www.chinstruments.com). All electrodes, unless otherwise stated, were tested in 30 mL of 1x PBS, with stirring. Increasing concentrations of H_2O_2 and glucose were added at 500 s intervals, unless otherwise indicated on a figure. Concentrations are reported in the total concentration of analyte in solution for a given time period.

Data processing

All statistical analysis and graphing was performed using GraphPad Prism 7 software (www.graphpad.com), unless otherwise specified. To evaluate the electroactive surface area (ESA), the peak current values from the CV results were used to solve the Randles-Sevcik equation. [5] The limit of detection (LoD) of the electrodes was calculated using 3σ methods. Rct values for impedance graphs were determined by fitting EIS data sets to an equivalent circuit model using the Nelder-Mead algorithm in the EIS Spectrum Analyzer software (http://www.abc.chemistry.bsu.by/vi/analyser/). Please see ESM for further details on calculations and data presentation and processing.

Results

Two distinct carbon-based laminate materials were produced and evaluated for their effectiveness as stamped laminate electrodes. The chemical preparation of the raw materials resulted in an eGR material that rapidly (~10 s) expanded into 'graphite worms', while minimal expansion was observed in the nGN. Expansion volume of intercalated graphite during heating has been demonstrated to be critical for generating high quality multi-layer laminates [35, 40]. The nGN material experienced comparably less expansion due to the starting nano-dimensions, which left far fewer layers of material to intercalate with sulfur during chemical exfoliation. This also affected compression of the material during preparation of the laminate electrodes as reduced volume in the graphitic worms resulted in poor compression and formation of a laminate when manual pressure was applied during the stamping process. It was noted that incomplete washing and drying of the eGR material resulted in slower, reduced expansion into vermiform structures (see movies in ESM Files S3–4). Freshly expanded eGR or nGN was used to produce stamped electrode laminates from each material. Electrodes produced on PET with eGR with spray adhesive were of consistent quality and maintained better adhesion to the substrate during testing, as compared to their counterpart nGN laminates. Electrodes made using Elmer's School Glue Stick can be lifted off the substrate, by dissolving the underlying glue in water (Fig. S2).

The described method was useful for measuring the amount of eGR used to make an electrode. The technique may also be used to deposit electrodes on materials that are fragile and prone to breaking under excessive pressure. Three replicate electrodes were created using the described method and an average mass of 8.03 mg ± 0.65 eGR per electrode was determined. Due to the low tensile strength of the nGN laminates, electrodes cannot be lifted off the substrate without disintegrating. Therefore, the mass of nGN required to fabricate an electrode was not accurately determined.

The method described (shown in Scheme 1) to produce electrode laminates is divided into a preparatory phase, in which the chemical treatment and wash steps are performed, the 3D mold and stamp is printed, and adhesive stencils are cut. The fabrication phase demonstrates the process for making the electrode (ESM File S6), where the adhesive stencil is applied to substrate, eGR or nGN material is used to fill the mold, and the laminate electrodes are made by pressing with the complementary stamp piece. Using an adhesive stencil on top of the substrate improved resolution of the electrode borders after removing the 3D printed mold. Despite the stencil, the edges of the electrodes were jagged, which was a result of the material being pressed in between the mold and the stamp. While this created minor inconsistencies between electrodes, the stability of the eGR electrodes in solution was excellent during testing as no graphitic material came loose. The electrodes produced with the nGN material had improved feature resolution as compared to the eGR electrodes, but the lack of complete compression of the material caused instability of the laminate during testing in solution. This was attributed to the flake size of the nGN material, as smaller flakes have been demonstrated to result in laminates with lower tensile strength [41], which explains why occasionally pieces of the nGN laminate came loose during testing. Attempts to further improve the resolution of the eGR electrodes resulted in smoother electrode topology after the electrode was re-pressed in between two pieces of smooth PET substrate. The same process of re-pressing was also tested on the nGN electrodes to attempt to increase their stability in solution, however, because the process presented here is limited to manual pressure, no noticeable improvement in electrode resolution or stability was observed. Despite this minor setback, the performance of both the eGR and nGN stamped laminate electrodes is evaluated throughout, as the eGR has better stability in solution, but the nGN had increased sensitivity to analytes. Thus, target application should be considered before selecting one material over another. It is also likely that the stability barrier of the nGN can be largely overcome by increasing the pressure applied during laminate fabrication as is done when producing large rolls of graphite foil, or by modifying the surface of the nGN electrodes with a stabilizing agent such as Nafion™ [42].

Physical characterization methods

Post fabrication, the sheet resistance of electrodes was measured from end to end (~30 mm) to determine the quality of fabrication, as well as the consistency between electrodes produced (Fig. S3). Numerical values of the sheet resistance measurements are reported in Table S1. The eGR laminates (Fig. S3b) had the lowest resistance and standard deviations

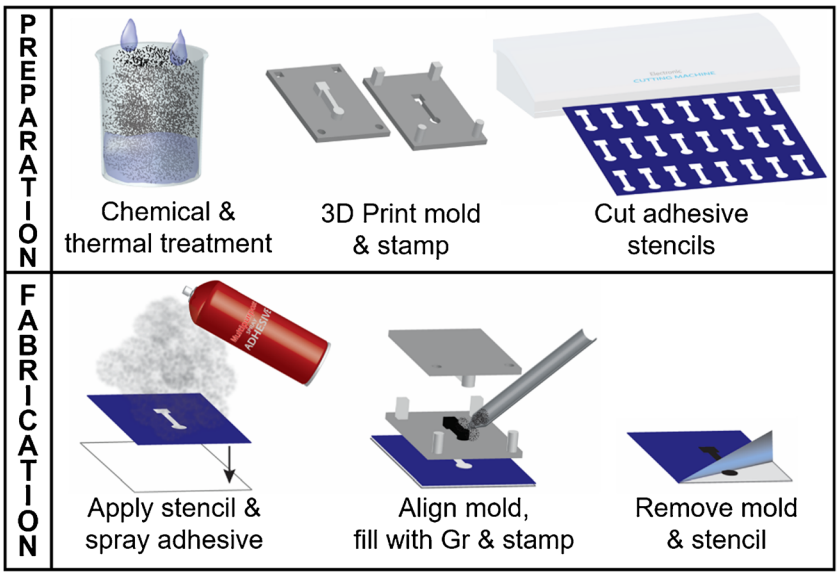

Scheme 1 Illustration of the process for creating compressed graphite laminate electrodes. Preparation phase: the raw graphite or nanographene material undergoes a series of chemical treatments and washing. A 3D printed mold and its complementary stamp are designed and printed, and adhesive stencils are cut out from single-sided adhesive paper. Fabrication phase: the substrate is cleaned and adhesive stencil is applied, followed by application of a thin layer of spray adhesive. The 3D printed mold is then aligned on the substrate and filled with expanded graphitic material (Gr), and the complementary stamp is pressed into the mold. The stamp and adhesive stencil are removed to reveal an electrode.

(8.0 Ω ± 1.0, $n = 3$) while the nGN laminates (Fig. S3c) had more than 5x higher sheet resistance than that of the eGR laminates (42.0 Ω ± 10.3). This was expected as the heterogenous size distributions in the nanoplatelet material cause alignment variations and gaps during the stamping process, whereas the large worm-like eGR pieces compressed easily due to overlapping, thereby creating a stable laminate with lower sheet resistance. Additionally, Reynolds et al., indicated that the expansion volume of the graphitic materials is directly related to the quality of the laminates produced [35]. Therefore, materials like nGN do not yield high-tensile strength laminates [41] due to smaller flake size, which results in reduced compression during stamping, and lower stability in solution.

The desire to put sensors on flexible and biodegradable materials is forefront in current wearable sensing technology. Therefore, in addition to measuring the resistance on PET substrates, eGR laminates were constructed on different flexible materials such at chitosan films (Fig. S3d-e) and polyimide (Fig. S3f) as these are candidates for wearable sensing applications. For quality control the resistance of commercial SPC electrodes (Zensor brand, Fig. S3g) was compared to that of eGR and nGN laminates. While the standard deviation of the control (SPC electrodes) measurements was only slightly elevated compared to eGR electrodes, the resistance measurements were significantly higher than the rest of the electrodes measured (73.5 Ω ± 1.8), indicating that the conductivity of the laminates was an improvement over that of the SPC electrodes.

Since the flexibility of the substrate is critical for wearable applications, the laminate material should also be flexible, without compromising device performance. To examine the suitability of the materials for flexible sensing applications, the sheet resistance of electrodes on polyimide substrates was measured before and after folding (Fig. S3f). Despite folding the electrodes in half, no significant difference in the resistance (Fig. S3a, pre-bend and post-bend) was observed, indicating that the flexibility of eGR laminates can be used for wearable sensing technologies. Laminates produced from nGN cannot be folded without compromising electrode conductivity. The electrodes on the chitosan films (Fig. S3d-e) were also amenable to mild bending, however, completely folding the films in half caused the substrates to break.

SEM was used to characterize the surface topography of the materials and electrodes (Fig. 1). The carbon-based materials, after chemical processing and thermal expansion, looked markedly different (Fig. 1a,d) as the difference between the eGR and nGN materials was visible to the naked eye. The difference on the microscale was evaluated using SEM to view the loose materials (Fig. 1b,e) as well as the material after it had been stamped into an electrode laminate (Fig. 1c,f). The thermally expanded (exfoliated) eGR flakes were vermiform in appearance, as previously described [35], with the typical eGR worm measuring between 1 and 3 mm across (Fig. 1b). The nGN worms were not prevalent, and measured less than ~500 μm (Fig. 1e). While the majority of the eGR had expanded into the worm shapes, the nGN material was comprised mostly of small pieces of graphitic material. Upon closer inspection (Fig. 1b,e insets), it was confirmed that the eGR worms as well as the smaller pieces of nGN were made up of sheets of graphene. When the expanded eGR materials were pressed together into laminate sheets, they maintained many of the desirable properties of their base single-layer graphene such as high conductivity and flexibility, combined with the desirable properties of laminates which enable them to be formed or cut [33, 43].

Spectroscopic characterization

To analyze the structure of the materials as well as the surface molecular groups, the electrodes were evaluated with Raman spectroscopy and XPS. The results from Raman spectroscopy (Fig. S5a) revealed the classic peaks between 1000 and 3000 cm^{-1} that are associated with primary carbon systems [44]. The lack of broadening of the 2D peak into 2D sub-peaks commonly associated with graphite also indicates that the graphite was of high quality [44], which was confirmed by the sharp peaks seen in x-ray powder diffraction analysis (Fig. S5b). The I_D/I_G ratios provide a sensitive measure of disorder, and the corresponding values were determined to be 0.05 ± 0.02 and 0.15 ± 0.07 for the nGN and eGR samples, respectively. Interestingly, the relatively low I_D/I_G ratio in both samples indicates a low number of structural defects in the samples. As Raman images were collected at two different regions on each sample, it is important to note that this was most likely not a localized effect as minimal variance was noted between the distinct locations on the electrodes. XPS was used to determine surface functional groups (Fig. S4) on the eGR laminates. The eGR analysis indicated that the most prominent peak was that of 1 s graphitic carbon, present at 285 eV, as anticipated [45]. The additional peaks present between 286 and 289 eV, represent carboxyls, epoxides, and carbonyl groups, which are functional groups amenable to covalent modification with biorecognition agents.

Electrochemical characterization

The suitability of these materials for electrochemical testing was further evaluated by calculating the electroactive surface area (ESA) from CV peak currents, performed at 5 $mV \cdot s^{-1}$ in the presence of a 4.0 mM ferro/ferricyanide redox couple (Fig. S6). CVs were also performed for electrodes over two ranges of applied potentials and five different scan rates to assess shifting of the oxidation peaks (Fig. S7). The CV of the eGR electrodes exhibited good performance over the range of −0.2 V to 0.6 V with very little shifting of the oxidation and reduction peaks at increasing scan rates (Fig. S7a,d).

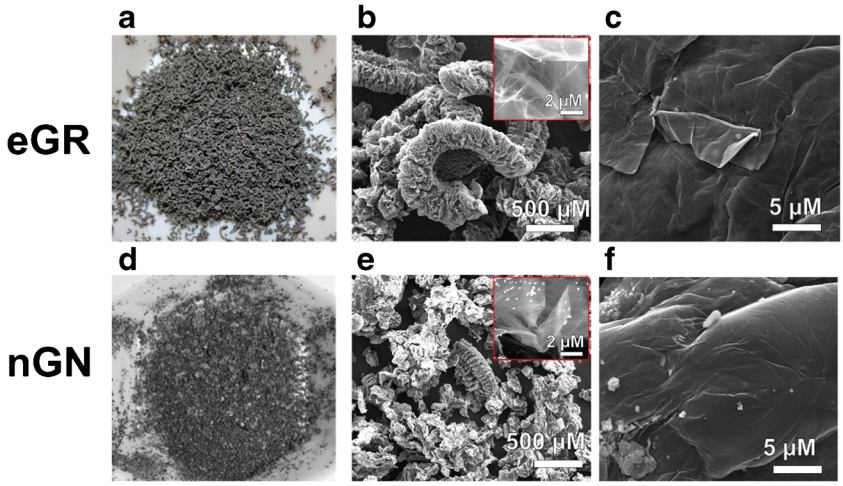

Fig. 1 Analysis of thermally expanded and compressed graphitic materials. Top row: eGR material **a** Loose eGR material. The size difference in the expanded materials is evident to the naked eye, as individual pieces of eGR can be readily discerned. **b** Scanning electron micrographs of loose eGR material, scale bar = 500 μm. Graphitic worms are quite large, extending over 1.0 mm in some cases. Inset shows a magnified view (5000x, scale bar = 2 μm) of the loose material where it becomes possible to see the graphene layers that make up the bulk material. **c** SEM of a stamped eGR laminate electrode, scale bar 5 = μm. Overlapping edges of the compressed material can be visualized in the image. Bottom row: nGN material **d** Bulk expanded nGN loose material. nGN particles are too small to readily differentiate from each other except on the periphery of the bulk material. **e** SEM of expanded nGN loose material, scale bar = 500 μm. Inset shows a magnified view (5000x, scale bar = 2 μm) of the loose material. The edges of graphene sheets that make up the bulk material are visible, along with residual contaminants from the chemical processing steps, indicating that washing does not completely remove chemicals such as phosphorous and potassium. **f** SEM of stamped nGN laminate electrode, scale bar = 5 μm. Small particles appear more frequently in the SEMs of stamped nGN as the material does not compress to the same degree as eGR, and the efficiency of the washing step is compromised by the small particle sizes

However, shifting and broadening of the peaks was seen in the CVs of nGN (Fig. S7b,e) indicating poor reversibility of the reaction on these electrodes. Additionally, multiple peak shapes were noted in the nGN CV which may be an effect of permanganate-oxidized graphene, indicating that a reduced potential range should be used during testing [46]. To evaluate all electrodes under the same conditions and calculate the ESA, a range of −0.4 to 1.0 V was selected, which also allowed for ESA analysis of the SPC electrodes. Using this method, it was determined that the nGN electrodes had the greatest average electroactive surface area (249 mm^2, calculated from peak 1) followed by the eGR electrodes (61.8 mm^2, calculated from peak 2), and the screen-printed carbon electrodes (13.2 mm^2). The CVs of the eGR and nGN electrodes were also recorded after treatment with PtNPs [(+) or (−) PtNPs on Fig. S6]. In both cases the treatment with platinum resulted in activity of the electrode over a larger range of current (dotted lines on Fig. S6). Calculations of the ESA also yielded higher values after treatment with PtNPs (nGN = 359 mm^2, eGR = 87.4 mm^2). The nGN laminate had the highest ESA due to the increased number of nanoscopic flakes present in the material, which resulted in more edge planes and faster heterogenous charge transport. The highly compressed eGR laminate had less surface area exposed to the redox solution and therefore had a lower ESA. However, the eGR had a charge transfer resistance (Rct) (Rct = 68.5) very similar to that of the nGN (Rct = 65.25) electrodes. SPC electrodes had a significantly high Rct value of 107. Very minimal diffusion limiting behavior was noted in the eGR and nGN electrodes, but the SPC electrodes had significant limitations due to diffusion. After treatment with platinum the Rct of eGR significantly decreased (down to 49.9), but the nGN remained the same. The diffusion limited region of the plot was also diminished for the eGR electrodes which supports the theory that the PtNPs increased the active surface area of the laminate. The lack of ESA increase in the nGN electrodes can be explained by the degradation of the electrodes during the platinum treatment. During electrodeposition, it is possible to see the nGN laminate physically degrade due the physical effects of oxygen bubbling at the surface. This degradation of some superficial graphene particles appears to improve the ESA with relatively no change in Rct.

Peroxide and glucose testing

To investigate the potential sensing capability of the eGR laminate materials, two different surface treatments were used (deposition of platinum nanoparticles and covalent modification with glucose oxidase). Peroxide sensing of untreated eGR electrodes was first measured at four potentials (0.2 V, 0.3 V, 0.4 V, and 0.5 V) to determine the best balance between signal response and background noise (Fig. S8). Higher or unpredictable levels of noise can limit the ability to accurately discriminate signal changes. A potential of 0.3 V (vs. Ag/AgCl)

yielded the best balance between electrode sensitivity and lowest overall background noise (Fig. S8). The amperometric response of untreated (no PtNPs, plasma, or GOx) eGR, nGN, and SPC electrodes was then evaluated using H_2O_2 detection as a model benchmark test (Fig. 2a and b). Response to increasing H_2O_2 concentrations, with H_2O_2 additions occurring every 500 s, was plotted as current (μA) versus time. Values for the total cumulative concentrations of analyte at each time point are available in Table S2. Sensitivity of the electrodes was determined by plotting current versus analyte concentration and identifying the slope of the linear sensing range of the data and dividing by the ESA. Out of the two laminates, the nGN electrodes had the highest signal amplitude at the higher concentrations of H_2O_2 (sensitivity = 29.2 $nA{\cdot}\mu M^{-1}{\cdot}cm^{-2}$, LoD = 1.96 μM), which was most likely a result of the high surface area of the material [13]. Laminates produced from eGR had a comparably attenuated signal at high H_2O_2 levels (sensitivity 34 $nA{\cdot}\mu M^{-1}{\cdot}cm^{-2}$) with a similar LoD = 1.95 μM. The SPC electrodes exhibited very poor sensitivity to H_2O_2 (7.2 $nA{\cdot}\mu M^{-1}{\cdot}cm^{-2}$) and a significantly higher LoD (235 μM). As platinum is known to catalyze the oxidation of H_2O_2, it is often used to increase the sensitivity of H_2O_2 and GOx-based sensors [47–49]. Electrodes were thus subjected to electrodeposition of PtNPs, and H_2O_2 sensing was repeated. The eGR electrodes had the greatest overall improvement in signal at higher concentrations, though the LoD was only slightly improved from (1.95 μM to 1.91 μM). However, the sensitivity of the electrode nearly doubled (64.3 $nA{\cdot}\mu M^{-1}{\cdot}cm^{-2}$). This indicates that the addition of PtNPs to eGR may not be beneficial for detection of low levels of H_2O_2, but increases in signal step sizes at higher concentrations are dramatically improved. Contrary to anticipated results, the overall amplitude decreased for the nGN electrodes after PtNP deposition (Fig. 2b) and sensitivity of the electrode was halved (16.55 $nA{\cdot}\mu M^{-1}{\cdot}cm^{-2}$ and LoD = 1.98 μM). These effects were further investigated using SEM (Fig. S9g, red arrows) to visualize the surface. SEMs revealed that portions of the nGN surface material had flaked off during treatment with PtNPs or during testing. Thus, reduced sensing capability was most likely a direct result of the lower tensile strength of the nGN laminate which caused the material to degrade during electrodeposition. As mentioned previously, increased amounts of platinum, or modification with a stabilizing polymer such as Nafion™ [42] would most likely stabilize the nGN structures on the surface. However, increased surface modification may compromise (or improve) attachment of biomolecules such as GOx. Alternatively, increases in surface modification may negatively affect background

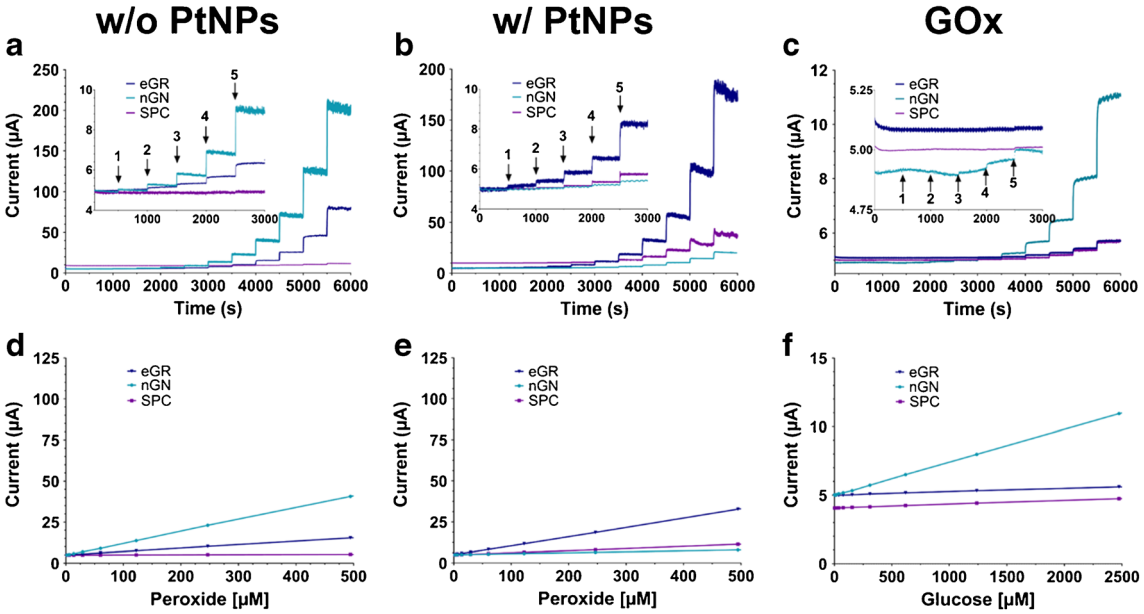

Fig. 2 Amperometric response of eGR, nGN, and SPC electrodes to H_2O_2 and glucose spikes at a potential of 0.3 V vs. ref. Ag/AgCl [0.1 M]. Increasing concentrations of H_2O_2 or glucose spikes were added every 500 s. **a** Time dependent response of electrodes to H_2O_2 without electrodeposited platinum nanoparticles (w/o PtNPs). Inset displays the response at lower levels of H_2O_2. Arrows 1–5 correspond to the total concentration of analyte in solution. 1.95, 5.85, 13.6, 29.2, 60.3 μM H_2O_2, respectively. These concentrations are also documented in Table S2. **b** Response of electrodes to H_2O_2 after electrodeposition of PtNPs. Analyte concentrations indicated by arrows correspond to those reported in (**a**). **c** Amperometric response of electrodes to glucose when functionalized with PtNPs and GOx. Inset: shows the response of electrodes at low levels of glucose concentrations. Increasing glucose concentrations correspond with increasing numerical arrows values. (1.22, 3.66, 8.52, 18.25, 37.69 μM respectively). Signals in plot **c** have been offset to allow for better visualization. **d-f** Linear calibration plots of current vs. concentration of analyte. Plots were generated from graphs a-c using the method described in the ESM. Calibration plots for, **d-e** H_2O_2 between 1.95–500 μM H_2O_2, and f 1.22 μM– 2.5 mM glucose. Linear regression analysis with 95% confidence interval of slope for each calibration plot is available in Table S3

noise of the electrode and delay stabilization in the testing solution. Despite this, the H_2O_2 sensing response of the electrodes was less than 10.0 s for both eGR and nGN and demonstrated good adherence to a linear trend between 2 and 500 μM H_2O_2 ($R^2 \geq 0.99$, see calibration plots in Fig. 2d-f, and linear regression analysis in Table S3). Of note, was the improvement in detection capability of the SPC electrodes (LoD from 235 μM down to 1.94 μM) after deposition of PtNPs. Since the geometric and electroactive surface area of the SPC electrodes was quite low (13.2 mm^2), the attachment of PtNPs actually serves to increase the effective surface area, and the LoD was improved. This significant increase in H_2O_2 sensitivity was not observed in the laminates as they had significantly higher starting ESA(s) than the SPC electrodes.

The final surface treatment of the electrodes investigated the potential use of these laminates as a platform for biosensing applications. To detect glucose, the enzyme GOx was attached to the working surface using covalent EDC/NHS amine-linker chemistry. Initially, this was tested in the absence of PtNPs or oxygen plasma treatment (Fig. S12), but results suffered from instability of signal and unpredictable noise. Since, plasma treatment is a recognized method for increasing the efficacy of covalent modification with biomolecules [20], PtNP-treated electrodes were exposed to oxygen plasma to enrich the surface with oxygen groups, prior to attachment of the enzyme GOx. The nGN laminates detected the lowest changes in glucose concentrations between 0 and 2.5 mM, with a LoD = 1.22 μM. Beyond 2.5 mM, the performance of the sensor was no longer linear, as larger amplitudes in step increases resulting from increasing levels of glucose (up to 9.88 mM), quickly took the shape of an exponential function. As the normal range for blood glucose is roughly ≤5 mM for healthy individuals [36, 50], and up to 33.3 mM in patients with hyperosmolar syndrome [51], the nGN laminates may be better suited to fluids with lower physiological levels of glucose. This includes fluids considered to be collected non-invasively, such as sweat (1–5 μM) [37], tears (75 μM) [38], or saliva (75 μM) [39]. These sample types have been demonstrated to have significantly lower glucose levels, but are still indicative of a diseased state [39, 52, 53]. The amplitude of signal response for eGR laminates to glucose was attenuated as compared to nGN electrodes, with a limit of detection of 18.5 μM glucose, and a linear trend between 0 and 5 mM (Fig. 2f, and Fig. S10), which demonstrated improvement over that of SPC. SPC electrodes lack the basal and edge planes of graphene that are inherently rich in oxygen and epoxide groups [54], and despite treatment with oxygen plasma, the attachment of GOx was compromised as a result. This caused a higher LoD for glucose (29.3 μM), and indicated that the laminate electrodes allow for improved glucose detection capability over the SPC electrodes both because of their higher surface area, as well as the surface oxygen moieties after treatment with plasma. This is also they reason why despite decreased sensitivity, nGN electrodes still had better glucose detection capability than eGR laminates. The nanoplatelet graphene has much more surface area made up of graphene edge planes which facilitates improved attachment of GOx. However, this was not tested due to the low stability of the electrode in testing solution.

While the detection range of the eGR laminates falls within the target concentrations found in healthy donor blood (5 mM for healthy, and ~10 mM for metabolic disorders), the linear operating range of the eGR (and nGN) limits capability to determine higher concentrations found in diabetic patients. Though the goal was to create a process for rapid production of eGR electrodes, there are several steps that could be taken to improve detection limits and range for analytes. These include investigation of high-pressure compression to produce uniform laminates, as well as precision cutting of electrode shapes to minimize surface area and edge variation. Also, varying conditions for plasma treatment would require extensive experimentation with concomitant identification of the best metal oxide for optimal catalytic activity, and finding the appropriate pH range for enzyme activity. It is also important to note that the commonly accepted practice for determining LoD still encourages the notion that a linear trend is superior compared to non-linear results. Therefore, calculations for sensitivity and LoD that use linear regression models should be subject to the parameters for these functions. However, the ideal conditions that govern biochemical models are often not followed in real testing applications. Thus, models such a Michaelis-Menten, Lineweaver-Burk, Hanes-Woolf, and Eadie-Hofstee are frequently being replaced by non-linear regression [55–58], particularly as computers become smaller and more powerful, and regression software more readily available. By incorporating these types of calculations and curve fitting, the sensitivity of these electrodes along with many other sensors could be dramatically improved. Though a caveat of parametric functions that use extrapolation to determine concentrations outside the known operating range require extensive calibration to reliably define the upper and lower maximums of operation [56, 59]. Beyond sensing applications, enzymatic conversion of biofuel is also a potential application for these laminates, as increased surface area facilitates increased concentrations of attached enzyme to allow for higher rates of conversion and energy production. Furthermore, the baseline capabilities of H_2O_2 sensing of the materials lends them to industrial applications of sensing, as H_2O_2 is now heavily used as a disinfectant in pharmaceutical, medicinal, cosmeceutical and household cleaning products [60].

Peroxide testing on flexible substrates

To verify the performance of eGR and nGN laminates on biodegradable substrates, the multi-layer graphene electrodes were fabricated on substrates with two different ratios of PCL/Agar [1:1 ratio, (1.9 mm and 1.1 mm thick) and 3:1 ratio,

(0.7 mm and 0.5 mm thick)], treated with platinum (Fig. 3) and tested with H_2O_2. The performance of electrodes on 2% $w{\cdot}v^{-1}$ dried chitosan, and polyimide films was also investigated. The eGR electrodes on PCL/Agar and chitosan substrates yielded promising signals, but the variability of the signal (nearly 70 μA at the highest concentration of H_2O_2) on the PCL/Agar films between different compositions of substrate indicates that method of creating the films may affect surface roughness and potentially the fabrication method. The films made from the 3:1 ratio of PCL/Agar were 3D printed, and thus had more surface roughness than those of the 1:1 ratio which were melted into a smooth mold. Interestingly enough, the melted materials had an increased response compared to the 3D printed materials, but the background noise on these electrodes was greater, therefore decreasing signal to noise ratios. Since the PCL/agar substrates where not perfectly smooth and level, an alternative method to put laminate electrodes on these materials would be to fabricate them via the lift off method and simply adhere them to the substrate using a water-insoluble glue. Out of the flexible substrates examined, the eGR electrodes on chitosan had the best response, but individual tests also demonstrated high noise levels, which was attenuated in the presented plot (Fig. 3) by the averaging of multiple runs. However, it was speculated that the increased signal in the chitosan electrodes was due to delamination of the chitosan film away from the eGR laminate (Fig. S11f). As the chitosan absorbs water from the testing solution, the film expands and peels away from the eGR, thereby leaving two sides of the electrode exposed, which increases the ESA, but also the signal variability between tests. Despite being suspended in solution agitated with a stir bar, the eGR that delaminated away from the chitosan remained intact with no observed physical degradation during testing, which has important implications for increasing surface area and improving sensitivity. The eGR electrodes on flexible polyimide tape performed the best out of the electrodes on alternative substrates, with an average ($n = 3$) of ~50 μA increase over that of the highest PCL/agar electrode. However, the sensors had reduced adherence to linear sensing trends (as compared to PET substrates) between 0 and 2 mM H_2O_2, with the lowest $R^2 \geq 0.83$ (for chitosan). The chitosan substrates yielded high variability between tests due to delamination of the electrodes, which resulted in high standard deviations and low R^2 values. As flexible substrates are increasingly important to the growing wearable sensing market, stability of the eGR laminates on polyimide is a promising step towards decreasing the cost of sensors. Moreover, the adaptation of the laminates onto robust, inexpensive, and degradable substrates is a key advancement for translating sensors to fieldable applications, such as environmental monitoring or animal health assessment, especially as society moves away from the use of plastics.

Conclusions

Low cost electrodes are critical components for sensing. Current techniques for producing low cost carbon-based electrodes utilize conductive inks for high throughput printing. However, the inks require the use of binders and surfactants to suspend the materials in solution, and then post-print annealing at high temperatures to remove the binder components. By using chemically exfoliated graphite followed by thermal expansion, the high yield of expanded materials makes it possible to fabricate hundreds of electrodes at low cost with a stamping method, as opposed to purchasing inkjet printers or compression rolling devices necessary for other methods of laminate or electrode fabrication. Furthermore, the stamping method allows for the utilization of temperature sensitive and flexible substrates such as paper or plastic, which is economical and amenable to wearable sensing applications. For fragile and degradable substrates, electrodes can be generated using soluble glues and then lifted off to be later

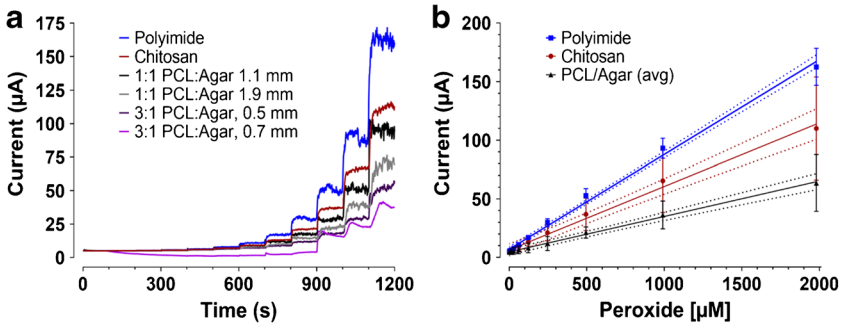

Fig. 3 Performance of eGR laminate electrodes on flexible and degradable substrates at an applied potential of 0.4 V. **a** Examination of the H_2O_2 sensing response of eGR electrodes on different substrates. Electrodes are treated with PtNPs. Substrates are 2% $w{\cdot}v^{-1}$ chitosan substrate ($n = 4$), PCL/Agar substrates of varying compositions and thickness ($n = 1$ for each substrate), and polyimide films, ($n = 3$). The description for fabrication of the substrates is described in the methods section. Thicknesses of the PCL:Agar laminate (1.1 mm, 1.9 mm, 0.5 mm, 0.7 mm) is indicated in the legend. Increasing concentrations of H_2O_2 were added every 100 s. Time dependent concentrations of H_2O_2 can be found in Table S2. **b** Linear trends of the averaged signals in plot **a**, with 95% confidence intervals plotted as dotted lines. Error bars indicate the standard deviation of the mean for each data set. Linear regression data for the slope of each line is available in Table S3

adhered to a backing of choice. As the need to create inexpensive disposable sensors is realized, the resulting waste from single use sensors should be a concern. This work helps address this issue by demonstrating performance of electrode laminates on inexpensive, 100% biodegradable substrates which can be thrown away, or left in the field after a test is completed. Finally, the ability to quickly synthesize the laminates to construct stamped electrodes with minimal equipment (3D printed mold is perhaps the most sophisticated part) means these electrodes can be produced in nearly any setting. The laminate electrodes performed well in baseline H_2O_2 and glucose testing models, though their linear range (1.22 μM – 2.5 mM) did not extend far enough to facilitate detection of higher levels of glucose in blood. As a result, the laminate electrodes may be best suited for research purposes or for non-invasive detection of low levels of glucose, such as those found in sweat, tears, or saliva. However, due to the endogenous peroxide sensing capabilities of untreated electrodes, the laminates can be used for industrial-based applications of peroxide detection, or other situations such as glucose-based fuel cells or detection of other low concentration target analytes. In summary, the presented techniques are a complete method for the production and testing of stamped multi-layer graphene laminate electrodes, which can be applied to virtually any substrate and used in a variety of research-grade sensing applications.

Acknowledgements We gratefully acknowledge funding support from the National Science Foundation under award number CBET-1706994 and ECCS-1841649, the National Institute of Food and Agriculture, U.S. Department of Agriculture, award numbers 2018-67011-27989 and 2016-67021-25038, and the Iowa State University Mechanical Engineering Departmental Fund. We would also like to thank Abraham Polonia-Suarez for his help with initial experiments.

Compliance with ethical standards The author(s) declare that they have no competing interests.

References

1. Kimmel DW, LeBlanc G, Meschievitz ME, Cliffel DE (2012) Electrochemical sensors and biosensors. Anal Chem 84(2):685–707. https://doi.org/10.1021/ac202878q
2. Sokolov AN, Roberts ME, Bao Z (2009) Fabrication of low-cost electronic biosensors. Mater Today 12(9):12–20. https://doi.org/10.1016/s1369-7021(09)70247-0
3. Renedo OD, Alonso-Lomillo MA, Martinez MJA (2007) Recent developments in the field of screen-printed electrodes and their related applications. Talanta 73(2):202–219. https://doi.org/10.1016/j.talanta.2007.03.050
4. Hayat A, Marty JL (2014) Disposable screen printed electrochemical sensors: tools for environmental monitoring. Sensors 14(6):10432–10453. https://doi.org/10.3390/s140610432
5. Brownson D, Banks C (2014) The handbook of graphene electrochemistry. Springer. https://doi.org/10.1007/978-1-4471-6428-9
6. Bollella P, Fusco G, Tortolini C, Sanzo G, Favero G, Gorton L, Antiochia R (2017) Beyond graphene: electrochemical sensors and biosensors for biomarkers detection. Biosens Bioelectron 89:152–166. https://doi.org/10.1016/j.bios.2016.03.068
7. Geim AK (2009) Graphene: status and prospects. Science 324(5934):1530–1534. https://doi.org/10.1126/science.1158877
8. Secor EB, Ahn BY, Gao TZ, Lewis JA, Hersam MC (2015) Rapid and versatile photonic annealing of graphene inks for flexible printed electronics. Adv Mater 27(42):6683–668+. https://doi.org/10.1002/adma.201502866
9. Celik N, Balachandran W, Manivannan N (2015) Graphene-based biosensors: methods, analysis and future perspectives. IET Circuits Dev Sys 9(6):434–445. https://doi.org/10.1049/iet-cds.2015.0235
10. Maduraiveeran G, Sasidharan M, Ganesan V (2018) Electrochemical sensor and biosensor platforms based on advanced nanomaterials for biological and biomedical applications. Biosens Bioelectron 103:113–129. https://doi.org/10.1016/j.bios.2017.12.031
11. Antiochia R, Tortolini C, Tasca F, Gorton L, Bollella P (2018) Chapter 1 - graphene and 2D-like nanomaterials: different biofunctionalization pathways for electrochemical biosensor development. In: Tiwari A (ed) Graphene bioelectronics. Elsevier, pp 1–35. https://doi.org/10.1016/B978-0-12-813349-1.00001-9
12. Ahmad R, Wolfbeis OS, Hahn Y-B, Alshareef HN, Torsi L, Salama KN (2018) Deposition of nanomaterials: a crucial step in biosensor fabrication. Materials Today Communications 17:289–321. https://doi.org/10.1016/j.mtcomm.2018.09.024
13. Pumera M, Sánchez S, Ichinose I, Tang J (2007) Electrochemical nanobiosensors. Sensors Actuators B Chem 123(2):1195–1205. https://doi.org/10.1016/j.snb.2006.11.016
14. Kitte SA, Gao W, Zholudov YT, Qi L, Nsabimana A, Liu Z, Xu G (2017) Stainless steel electrode for sensitive Luminol Electrochemiluminescent detection of H2O2, glucose, and glucose oxidase activity. Anal Chem 89(18):9864–9869. https://doi.org/10.1021/acs.analchem.7b01939
15. Miao X, Feng Z, Tian J, Peng X (2014) Glucose detection at attomole levels using dynamic light scattering and gold nanoparticles. SCIENCE CHINA Chem 57(7):1026–1031. https://doi.org/10.1007/s11426-014-5079-x
16. Guo X, Liang B, Jian J, Zhang Y, Ye X (2014) Glucose biosensor based on a platinum electrode modified with rhodium nanoparticles and with glucose oxidase immobilized on gold nanoparticles. Microchim Acta 181(5):519–525. https://doi.org/10.1007/s00604-013-1143-z
17. Martín-Yerga D, Carrasco-Rodríguez J, Fierro JLG, García Alonso FJ, Costa-García A (2017) Copper-modified titanium phosphate nanoparticles as electrocatalyst for glucose detection. Electrochim Acta 229:102–111. https://doi.org/10.1016/j.electacta.2017.01.143
18. Xu Q, Gu S-X, Jin L, Y-e Z, Yang Z, Wang W, Hu X (2014) Graphene/polyaniline/gold nanoparticles nanocomposite for the direct electron transfer of glucose oxidase and glucose biosensing. Sensors Actuators B Chem 190:562–569. https://doi.org/10.1016/j.snb.2013.09.049
19. Berger C, Song ZM, Li XB, Wu XS, Brown N, Naud C, Mayou D, Li TB, Hass J, Marchenkov AN, Conrad EH, First PN, de Heer WA (2006) Electronic confinement and coherence in patterned epitaxial graphene. Science 312(5777):1191–1196. https://doi.org/10.1126/science.1125925
20. Bilek MM, McKenzie DR (2010) Plasma modified surfaces for covalent immobilization of functional biomolecules in the absence of chemical linkers: towards better biosensors and a new generation of medical implants. Biophys Rev 2(2):55–65. https://doi.org/10.1007/s12551-010-0028-1
21. Ren J, Shi W, Li K, Ma Z (2012) Ultrasensitive platinum nanocubes enhanced amperometric glucose biosensor based on chitosan and

nafion film. Sensors Actuators B Chem 163(1):115–120. https://doi.org/10.1016/j.snb.2012.01.017

22. Mani V, Dinesh B, Chen S-M, Saraswathi R (2014) Direct electrochemistry of myoglobin at reduced graphene oxide-multiwalled carbon nanotubes-platinum nanoparticles nanocomposite and biosensing towards hydrogen peroxide and nitrite. Biosens Bioelectron 53:420–427. https://doi.org/10.1016/j.bios.2013.09.075
23. Qian J, Yang X, Yang Z, Zhu G, Mao H, Wang K (2015) Multiwalled carbon nanotube@reduced graphene oxide nanoribbon heterostructure: synthesis, intrinsic peroxidase-like catalytic activity, and its application in colorimetric biosensing. J Mater Chem B 3(8):1624–1632. https://doi.org/10.1039/C4TB01702A
24. Tran TS, Dutta NK, Choudhury NR (2018) Graphene inks for printed flexible electronics: graphene dispersions, ink formulations, printing techniques and applications. Adv Colloid Interf Sci. https://doi.org/10.1016/j.cis.2018.09.003
25. Hondred J, Stromberg L, Mosher C, Claussen J (2017) High resolution graphene films for electrochemical sensing via inkjet Maskless lithography. ACS Nano. https://doi.org/10.1021/acsnano.7b03554
26. Secor EB, Gao TZ, Islam AE, Rao R, Wallace SG, Zhu J, Putz KW, Matuyama B, Hersam MC (2017) Enhanced conductivity, adhesion, and environmental stability of printed graphene inks with nitrocellulose. Chem Mater 29(5):2332–2340. https://doi.org/10.1021/acs.chemmater.7b00029
27. Das S, Srinivasan S, Stromberg L, He Q, Garland N, Straszheim W, Ajayan P, Balasubramanian G, Claussen J (2017) Superhydrophobic inkjet printed flexible graphene circuits via direct-pulsed laser writing. Nanoscale Advance Article 9:19058–19065. https://doi.org/10.1039/C7NR06213C
28. Malekpour H, Chang KH, Chen JC, Lu CY, Nika DL, Novoselov KS, Balandin AA (2014) Thermal conductivity of graphene laminate. Nano Lett 14(9):5155–5161. https://doi.org/10.1021/nl501996v
29. Gao W, Singh N, Song L, Liu Z, Reddy AL, Ci L, Vajtai R, Zhang Q, Wei B, Ajayan PM (2011) Direct laser writing of micro-supercapacitors on hydrated graphite oxide films. Nat Nanotechnol 6(8):496–500. https://doi.org/10.1038/nnano.2011.110
30. Huang XJ, Leng T, Zhang X, Chen JC, Chang KH, Geim AK, Novoselov KS, Hu ZR (2015) Binder-free highly conductive graphene laminate for low cost printed radio frequency applications. Appl Phys Lett 106(20). https://doi.org/10.1063/1.4919935
31. Rinaldi A, Proietti A, Tamburrano A, Ciminello M, Sarto MS (2015) Graphene-based strain sensor Array on carbon Fiber composite laminate. IEEE Sensors J 15(12):7295–7303. https://doi.org/10.1109/jsen.2015.2472595
32. Huang XJ, Leng T, Georgiou T, Abraham J, Nair RR, Novoselov KS, Hu ZR (2018) Graphene oxide dielectric permittivity at GHz and its applications for wireless humidity sensing. Sci Rep 8. https://doi.org/10.1038/s41598-017-16886-1
33. Cai W, Lai T, Du H, Ye J (2014) Electrochemical determination of ascorbic acid, dopamine and uric acid based on an exfoliated graphite paper electrode: a high performance flexible sensor. Sens Actuators B Chem 193:492–500. https://doi.org/10.1016/j.snb.2013.12.004
34. Marcano DC, Kosynkin DV, Berlin JM, Sinitskii A, Sun ZZ, Slesarev A, Alemany LB, Lu W, Tour JM (2010) Improved synthesis of graphene oxide. ACS Nano 4(8):4806–4814. https://doi.org/10.1021/nn1006368
35. Reynolds RA, Greinke RA (2001) Influence of expansion volume of intercalated graphite on tensile properties of flexible graphite. Carbon 39(3):479–481. https://doi.org/10.1016/s0008-6223(00)00291-8
36. Martinkova P, Pohanka M (2015) Biosensors for blood glucose and diabetes diagnosis: evolution, construction, and current status. Anal Lett 48(16):2509–2532. https://doi.org/10.1080/00032719.2015.1043661
37. Sato K, Kang WH, Saga K, Sato KT (1989) Biology of sweat glands and their disorders. 1. Normal sweat-gland-function. J Am Acad Dermatol 20(4):537–563. https://doi.org/10.1016/s0190-9622(89)70063-3
38. Agustini D, Bergamini MF, Marcolino-Junior LH (2017) Tear glucose detection combining microfluidic thread based device, Amperometric biosensor and microflow injection analysis. Biosens Bioelectron 98:161–167. https://doi.org/10.1016/j.bios.2017.06.035
39. Jurysta C, Bulur N, Oguzhan B, Satman I, Yilmaz TM, Malaisse WJ, Sener A (2009) Salivary glucose concentration and excretion in Normal and diabetic subjects. J Biomed Biotechnol. https://doi.org/10.1155/2009/430426
40. Chung DDL (2016) A review of exfoliated graphite. J Mater Sci 51(1):554–568. https://doi.org/10.1007/s10853-015-9284-6
41. Gu JL, Leng Y, Gao Y, Liu H, Kang FY, Shen WN (2002) Fracture mechanism of flexible graphite sheets. Carbon 40(12):2169–2176. https://doi.org/10.1016/s0008-6223(02)00075-1
42. Lu J, Drzal LT, Worden RM, Lee I (2007) Simple fabrication of a highly sensitive glucose biosensor using enzymes immobilized in exfoliated graphite Nanoplatelets Nafion membrane. Chem Mater 19(25):6240–6246. https://doi.org/10.1021/cm702133u
43. Dikin DA, Stankovich S, Zimney EJ, Piner RD, Dommett GHB, Evmenenko G, Nguyen ST, Ruoff RS (2007) Preparation and characterization of graphene oxide paper. Nature 448(7152):457–460. https://doi.org/10.1038/nature06016
44. Ferrari AC (2007) Raman spectroscopy of graphene and graphite: disorder, Electron-phonon coupling, doping and nonadiabatic effects. Solid State Commun 143(1–2):47–57. https://doi.org/10.1016/j.ssc.2007.03.052
45. Lotya M, Hernandez Y, King PJ, Smith RJ, Nicolosi V, Karlsson LS, Blighe FM, De S, Wang ZM, McGovern IT, Duesberg GS, Coleman JN (2009) Liquid phase production of graphene by exfoliation of graphite in surfactant/water solutions. J Amer Chem Soc 131(10):3611–3620. https://doi.org/10.1021/ja807449u
46. Ambrosi A, Chua CK, Latiff NM, Loo AH, Wong CHA, Eng AYS, Bonanni A, Pumera M (2016) Graphene and its electrochemistry - an update. Chem Soc Rev 45(9):2458–2493. https://doi.org/10.1039/c6cs00136j
47. Malekzad H, Sahandi Zangabad P, Mirshekari H, Karimi M, Hamblin Michael R (2017) Noble metal nanoparticles in biosensors: recent studies and applications. Nanotechnol Rev 6:301–329. https://doi.org/10.1515/ntrev-2016-0014
48. Hrapovic S, Liu Y, Male KB, Luong JHT (2004) Electrochemical biosensing platforms using platinum nanoparticles and carbon nanotubes. Anal Chem 76(4):1083–1088. https://doi.org/10.1021/ac035143t
49. Saei AA, Dolatabadi JEN, Najafi-Marandi P, Abhari A, de la Guardia M (2013) Electrochemical biosensors for glucose based on metal nanoparticles. TrAC Trends Anal Chem 42:216–227. https://doi.org/10.1016/j.trac.2012.09.011
50. Hayashino Y, Fukuhara S, Suzukamo Y, Okamura T, Tanaka T, Ueshima H (2007) Normal fasting plasma glucose levels and type 2 diabetes: the high-risk and population strategy for occupational health promotion (HIPOP-CHP) study. Acta Diabetol 44(3):164–166. https://doi.org/10.1007/s00592-007-0258-2
51. Rosenbloom AL (2010) Hyperglycemic hyperosmolar state: an emerging pediatric problem. J Pediatr 156(2):180–184. https://doi.org/10.1016/j.jpeds.2009.11.057
52. Lee Y-H, Wong DT (2009) Saliva: an emerging biofluid for early detection of diseases. Am J Dent 22(4):241–248

53. Gao W, Emaminejad S, Nyein HYY, Challa S, Chen KV, Peck A, Fahad HM, Ota H, Shiraki H, Kiriya D, Lien DH, Brooks GA, Davis RW, Javey A (2016) Fully integrated wearable sensor arrays for multiplexed in situ perspiration analysis. Nature 529(7587): 509–50+. https://doi.org/10.1038/nature16521
54. Ganguly A, Sharma S, Papakonstantinou P, Hamilton J (2011) Probing the thermal deoxygenation of graphene oxide using high-resolution in situ X-ray-based spectroscopies. J Phys Chem C 115(34):17009–17019. https://doi.org/10.1021/jp203741y
55. Duggleby RG (1995) [3] analysis of enzyme progress curves by nonlinear regression. In: Methods in enzymology, vol 249. Academic Press, pp 61–90. https://doi.org/10.1016/0076-6879(95)49031-0
56. Leatherbarrow RJ (1990) Using linear and non-linear regression to fit biochemical data. Trends Biochem Sci 15(12):455–458. https://doi.org/10.1016/0968-0004(90)90295-M
57. Stroberg W, Schnell S (2016) On the estimation errors of KM and V from time-course experiments using the Michaelis–Menten equation. Biophys Chem 219:17–27. https://doi.org/10.1016/j.bpc.2016.09.004
58. Yagati AK, Pyun J-C, Min J, Cho S (2016) Label-free and direct detection of C-reactive protein using reduced graphene oxide-nanoparticle hybrid impedimetric sensor. Bioelectrochemistry 107:37–44. https://doi.org/10.1016/j.bioelechem.2015.10.002
59. Motulsky H, Christopoulos A (2004) Fitting models to biological data using linear and nonlinear regression: a practical guide to curve fitting. Oxford University Press
60. Mani V, Govindasamy M, Chen S-M, Chen T-W, Kumar AS, Huang S-T (2017) Core-shell heterostructured multiwalled carbon nanotubes@reduced graphene oxide nanoribbons/chitosan, a robust nanobiocomposite for enzymatic biosensing of hydrogen peroxide and nitrite. Sci Rep 7(1):11910. https://doi.org/10.1038/s41598-017-12050-x